View metadata, citation and similar papers at core.ac.uk
brought to you by CORE
provided by CERN Document Server

To appear in AJ
Preprint typeset using LaTeX style emulateapj

GLOBULAR CLUSTERS IN DENSE CLUSTERS OF GALAXIES[1]

John P. Blakeslee
Palomar Observatory, California Institute of Technology, Mail Stop 105-24, Pasadena, CA 91125
Electronic mail: jpb@astro.caltech.edu

To appear in AJ

ABSTRACT

Deep imaging data from the Keck II telescope are employed to study the globular cluster (GC) populations in the cores of six rich Abell clusters. The sample includes A754, A1644, A2124, A2147, A2151, and A2152 and covers the redshift range $z = 0.035$–0.066. These clusters also span a range in morphology from spiral-rich, irregular systems to centrally concentrated cD clusters rich in early-type galaxies. Globular cluster specific frequencies S_N and luminosity function dispersions $\sigma_{\rm LF}$ are measured for a total of 9 galaxies in six central fields. The measured values of S_N for the six brightest cluster galaxies (BCGs) are all higher than typical values for giant ellipticals, in accord with the S_N-density correlations found by Blakeslee, Tonry, & Metzger (1997). The three non-BCGs analyzed also have elevated values of S_N, confirming that central location is a primary factor. Two different models are used to estimate $\eta_{\rm GC}$, the number of GCs per unit mass, for these central cluster fields. The values for $\eta_{\rm GC}$ are consistent with those found in the earlier sample, again indicating that the number of GCs scales with mass and that the S_N variations are due to a deficit of halo light, i.e., S_N reflects mass-to-light ratio. The similarity of the GC color distributions of BCGs and more ordinary ellipticals further implies that no special mechanism is needed for explaining the properties of these GC populations.

The discussion builds on an earlier suggestion that the GCs (both metal rich and metal poor) around the central cluster galaxies were assembled at early times, and that star formation halted prematurely in the central galaxies at the epoch of cluster collapse. It is argued that this "BCG saturation" model is consistent with recent simulations of BCG/cluster formation. The subsequent addition of luminous material to the BCG through cluster dynamical evolution can cause S_N to decrease while conserving $\eta_{\rm GC}$, but both theory and observations indicate that the time scale for this is long. However, there may be some evidence of it in the present sample and elsewhere. Finally, the GC luminosity function measurements are used to constrain the relative distances of the three clusters that make up the Hercules supercluster.

Subject headings: galaxies: clusters: general — galaxies: elliptical and lenticular, cD — galaxies: star clusters — globular clusters: general

1. INTRODUCTION

Enormous populations of 10,000 or more globular clusters (GCs) surround the central giant galaxies in rich galaxy clusters. This was first noticed more than forty years ago in the case of M87 at the center of the Virgo cluster (Baum 1955). While a GC specific frequency S_N (number of GCs per unit $M_V = -15$ of galaxy luminosity; Harris & van den Bergh 1981) near 4 is typical for giant elliptical galaxies, some galaxies such as M87 have $S_N \sim 12$. Harris & Petrie (1978) concluded that either (1) the number of GCs scales with total mass and M87 has a mass-to-light ratio M/L that is 2-3 times higher than other giant ellipticals, or (2) local initial conditions at the center of the Virgo cluster stimulated M87 to form more GCs per unit mass.

Until recently, the sparse data available on the subject indicated that S_N for central cluster galaxies was uncorrelated with any other obvious galaxy or cluster properties (Harris, Pritchet, & McClure 1995; West et al. 1995). The puzzling variations in S_N among these galaxies was interpreted as reflecting local initial conditions, and therefore unpredictable from our current vantage point. Thus, the latter of Harris & Petrie's two explanations grew in popularity (e.g., Harris 1991; McLaughlin, Harris & Hanes 1994). A general trend of increasing S_N with environmental density was recognized, however, and various authors attempted to explain why galaxies in denser environments, and central cluster galaxies in particular, might have been more efficient in forming GCs (e.g., West 1993; Harris & Pudritz 1994).

A recent study of a complete sample of central galaxies in 19 Abell clusters within 10,000 km s^{-1} showed that, in contrast to the conclusions of previous works, S_N for these galaxies correlates well with overall cluster properties, including velocity dispersion, X-ray luminosity, and the local density of bright galaxies (Blakeslee 1997). This study used the method of Blakeslee & Tonry (1995), which combines information from the counts of faint point sources in the galaxy halos with measurements of the residual surface brightness variance after the galaxy and detected point sources are removed. The method allows for better constraints on the total number of GCs while simultaneously constraining the form of the GC luminosity function

[1]Based on observations obtained at the W.M. Keck Observatory, operated as a scientific partnership by the California Institute of Technology, the University of California, and the National Aeronautics and Space Administration. Keck Observatory was made possible by the generous financial support of the W.M. Keck Foundation.

(GCLF), which is of interest because of its frequent use as a standard candle distance indicator (see reviews by Harris 1991 and Whitmore 1996).

Blakeslee, Tonry, & Metzger (1997, hereafter BTM) showed that the observed S_N correlations were consistent with a simple model in which the number of GCs scales with mass rather than luminosity. (This was the alternative possibility raised by Harris & Petrie.) The GC formation efficiency, or the rate of GC formation per unit mass $\eta_{\rm GC} = N_{\rm GC}/M$, would therefore be universal. BTM found roughly $\eta_{\rm GC} \sim 0.7$ GC per $10^9\,M_\odot$. The observed correlations of central galaxy S_N with cluster density are then due to this scaling of GC number with mass in conjunction with the relative insensitivity of the present-day galaxy luminosity to cluster richness (e.g., Postman & Lauer 1995). This is the same phenomenon that makes these galaxies rough standard candles. Thus, rather than having anomalously large GC populations, these galaxies appear to be underluminous for their prominent positions in the centers of very rich clusters.

Blakeslee (1997) speculated that tidal disruption from the collapse of the surrounding cluster may have removed the star-forming gas and halted further luminosity growth in the central galaxy sometime after the GCs had formed. Harris, Harris, & McLaughlin (1998) suggested that protogalactic winds driven by a rapid initial starburst were what removed the gas and halted the luminosity growth. Building on this idea, McLaughlin (1999b) has compiled further evidence for a universal GC formation efficiency. These ideas do not conflict with evolutionary models in which GCs and other material are later stripped from the rest of the cluster members and added to the central galaxy (Muzzio 1987; Côté, Marzke, & West 1998).

The present work uses Keck imaging data to extend the BTM study to larger distances and higher density environments. Because the BTM observations were conducted on a 2.4 m telescope, the sample was limited to clusters within $z \lesssim 0.033$, and this limited the variety of clusters that could be studied. In fact, the richest in that sample was the Coma cluster, the very first one for which data were obtained (Blakeslee & Tonry 1995). Thus, although BTM found strong correlations of the central galaxy S_N with cluster properties, the full range of these correlations had yet to be explored. The sample of galaxies presented here extends twice as far in distance as the earlier sample.

The following section describes the selection and properties of the present sample of galaxies. Observations and data reductions are discussed in Section 3, which includes the radial number density distributions of the faint objects that cluster around the central galaxies. Section 4 presents the main results on the GC luminosity functions, specific frequencies, and inferred mass formation efficiencies. Section 5 then discusses the relevance of these results for formation and evolution models of GC populations and for estimates of the distances to these clusters. The final section provides a summary.

2. THE GALAXY SAMPLE

The goal of this program was to extend the BTM survey of GC populations in 23 giant elliptical galaxies (gE's) in 19 clusters to denser and more diverse environments. Because of practical considerations, the selected clusters are all in the northern spring sky and at redshifts $z < 0.07$. Table 1 summarizes the cluster X-ray, dynamical, and morphological properties. All X-ray information is due to Jones & Forman (1999). The velocity information comes from a variety of sources, including Zabludoff & Zaritsky (1995) for A754, Hill & Oegerle (1993) as modified by Fadda et al. (1996) for A2124, and Barmby & Huchra (1998) for A2147, A2151, and A2152. There are discordant values in the literature for the A1644 velocity dispersion. Struble & Rood (1991) quote $\sigma_{\rm cl} = 991$ km s^{-1} from 92 galaxies and Zabludoff et al. (1993) find 939^{+87}_{-68} km s^{-1} from 76 galaxies, but Fadda et al. (1996) find a gently falling velocity dispersion profile and quote an asymptotic value of 759^{+61}_{-56} km s^{-1} from 84 galaxies. The tabulated value of 890 km s^{-1} is found from a 3σ-clipped average of 63 galaxies from the NASA/IPAC Extragalactic Database (NED) within $1\,h^{-1}$ Mpc of the central galaxy.

There are also discrepant dispersion values published for A2147 and A2152, the two overlapping clusters that along with A2151 comprise the Hercules supercluster. Zabludoff et al. (1993) found $\sigma_{\rm cl} = 1081^{+170}_{-117}$ for A2147 and $\sigma_{\rm cl} = 1346^{+276}_{-173}$ for A2152 from 32 and 21 galaxy velocities, respectively; Barmby & Huchra (1998) find the much smaller tabulated values using 93 and 56 velocities, respectively. These latter authors employed a method of minimizing a vector that consisted of the two projected spatial dimensions and the velocity offset to unambiguously assign galaxies to individual clusters (or the "dispersed supercluster" component) in this complex region. This approach may tend to yield lower dispersion values but appears to be more consistent in giving mean velocities closer to the measured values for the respective central brightest cluster members. For instance, previous investigations generally found very similar redshifts for the three Hercules clusters, while Barmby & Huchra find that A2152 has a significantly higher mean velocity, close to that of its central galaxy (Postman & Lauer 1995).

The first three clusters in Table 1 are centrally concentrated Bautz-Morgan type I/II, Rood-Sastry type cD clusters dominated by a single giant galaxy, while the last three are less concentrated BM type III, RS type F clusters with more ordinary brightest members. The three Hercules clusters also have elevated spiral fractions, with that of A2151 being about 50% (Tarenghi et al. 1980), as compared to the 20-30% typical of rich clusters (Dressler 1980a,b). Since the velocity dispersions and (except for A754 and A2152) X-ray temperatures of all the sample clusters are fairly similar, the masses might also be similar. Thus, the observed morphological differences may be solely indicative of evolutionary state, and one might look for evolutionary effects in the GC populations.

Few of the central cluster galaxies in the present sample have been the subjects of photographic surface photometry studies that have classified them as "cD galaxies," meaning that they have extended envelopes with luminosities in excess of the $r^{1/4}$-law profiles defined by the inner parts (Oemler 1976). Moreover, the Rood-Sastry "cD" classification does not depend on having a central galaxy with this sort of significantly extended cD envelope. For instance, the bright central galaxy in the F-type cluster A2147 is classified as a cD galaxy (Schombert 1988). To avoid confusion, this paper will generally refer to the program galaxies as "central galaxies," or as "brightest cluster

TABLE 1
ABELL CLUSTER SAMPLE

Cluster	RA_X (J2000)	Dec_X	z_{CMB}	σ_{cl}	L_X	kT_X	R	BM	RS	Constellation
A754	9 09 04.3	−09 39 38	0.0552	900 ± 70	6.89 ± 0.10	9.1	2	I	cD	Hydra
A1644	12 57 19.3	−17 22 06	0.0485	890 ± 85	2.49 ± 0.03	4.7	1	II	cD	Virgo
A2124	15 45 00.4	+36 06 56	0.0660	880 ± 80	1.16 ± 0.05	3.5[e]	1	I	cD	Corona Borealis
A2147	16 02 15.3	+15 57 58	0.0354	820 ± 65	1.89 ± 0.02	4.4	1	III	F	Hercules
A2151	16 04 37.0	+17 43 40	0.0367	705 ± 45	0.88 ± 0.02	3.8	2	III	F	Hercules
A2152	16 05 37.8	+16 26 17	0.0434	715 ± 75	0.21 ± 0.02	1.9[e]	1	III	F	Hercules

[e]Estimated from the L_X–T_X relation of Jones & Forman (1999), which has an uncertainty of about 55%.

NOTE.—Table lists for each cluster: coordinates of the peak of the extended X-ray emission (Jones & Forman 1999); redshift in the cosmic microwave background rest frame; velocity dispersion (km s^{-1}); X-ray luminosity in the 0.5–4.5 keV band (10^{44} ergs/s) and X-ray gas temperature (keV) (Jones & Forman 1999); richness class and Bautz-Morgan type (Abell et al. 1989); Rood-Sastry type (Struble & Rood 1987); and the host constellation. See text for a discussion of the sources of the velocity information.

galaxies" (BCGs). As shown most notably by M87 in the Virgo cluster (and in other clusters discussed by BTM), the central cluster galaxy need not be the BCG; however, the BCGs are central for all of the clusters in the present sample.

3. OBSERVATIONS AND REDUCTIONS

Deep R-band images of the sample galaxies were obtained in April 1997 with the Low Resolution Imaging Spectrograph (LRIS) (Oke et al. 1995) on the 10 m Keck II telescope on Mauna Kea, Hawaii. The image scale was $0\farcs211$ pix^{-1} and the usable area was about $7\farcm2 \times 5\farcm5$. The median seeing was about $0\farcs65$. The moon was at last quarter, but conditions were photometric and several Landolt (1992) standard fields were observed for calibration. Independent photometry for four of the program fields was acquired at Palomar Observatory and agreed to within 0.02 mag in each case. Individual LRIS exposures were bias-subtracted, flat-fielded, and combined, rejecting cosmic ray hits, to produce the final images. Two amplifier readout was used, but otherwise this proceeded as detailed by BTM.

Table 2 provides a summary of the LRIS Abell cluster observations. The coordinates for the $z < 0.05$ BCGs come from Postman & Lauer (1995); the coordinates for the other two are from NED. The quantity m_1^* listed in the table is one measure of the depth of an observation and can be compared directly to the values listed by BTM. Formally, it corresponds to the magnitude of an object that is bright enough to produce one detected photoelectron per total image integration time, corrected for Galactic extinction. Thus, the extinction-corrected magnitude of an object yielding f total counts in the image is simply $m = -2.5\log(f) + m_1^*$. The $m_R^{50\%}$ quantity in the table gives a better measure of overall image quality; it corresponds to the extinction-corrected 50% completeness limit for object detection above a $4\,\sigma$ threshold. The numbers were determined from the completeness experiments discussed below.

Figures 1–6 (appended to end of paper) display the central $\sim 4\farcm2$ of the deep LRIS R-band images. The A2124 image shows the redshift $z = 0.57$ gravitationally lensed arc $27''$ to the southeast of the cD center (Blakeslee & Metzger 1999). To study the GC populations, we model and subtract the galaxy halo light then subtract the large-scale residuals before performing the point-source photometry and image power spectrum measurements. The reduction and analysis methods are described in detail by BTM and Blakeslee & Tonry (1995). The following subsections summarize the reduction procedure, highlighting the steps that had to be altered for the current data set.

3.1. *Point Source Photometry and Completeness*

LRIS has a spatially varying point spread function (PSF). When stellar images near the center of the chip are in focus, the images near the chip corners are significantly extended. The width of the PSF varies by as much as 15% across the chip; if unaccounted for, this could produce a photometry error of ~ 0.3 mag. BTM used a version of the photometry program DOPHOT (Schechter et al. 1993) that had been modified to account for additional noise from the galaxy light that had been modeled and subtracted. That version made no allowance for a variable PSF, so we instead used the version described by Metzger & Schechter (1998), and kindly provided by M. Metzger, that allows the PSF shape parameters to vary as a two-dimensional quadratic function of position on the CCD. We modified this version so that it also allowed for extra noise from the subtracted galaxy light and used an aperture correction that varied as an independent two-dimensional quadratic function of position. With the allowance made for the variable PSF, the fitted spatial variation of the aperture correction was typically less than 0.07 mag and always less than 0.1 mag. In the end, we disregarded all information on objects very near the CCD corners, more than about $3\farcm5$ from the center, where the stellar images were worst.

To test the accuracy of the object magnitudes, we did aperture photometry by hand (in the same way as for the Landolt standards) for about 15 of the brightest, relatively clean, unsaturated stars in each image. The results agreed at the 0.02 mag level with the DOPHOT magnitudes for all of the fields except A2124, for which the DOPHOT values

TABLE 2
KECK LRIS OBSERVATIONS OF CENTRAL CLUSTER GALAXIES

Field	RA (J2000)	Dec	l	b	A_R	Exp	PSF	sec z	m_1^*	$\mu_{\rm sky}$	$m_R^{50\%}$	m_R^0
A754	9 08 32.3	−09 37 48	239.20	+24.70	0.17	4600	0.84	1.28	37.19	20.9	26.4	28.9
A1644	12 57 11.8	−17 24 35	304.89	+45.44	0.18	6000	0.66	1.28	37.47	21.0	27.0	28.6
A2124	15 44 58.8	+36 06 35	57.76	+52.30	0.07	8400	0.57	1.10	37.96	20.7	27.3	29.3
A2147	16 02 17.0	+15 58 28	28.91	+44.52	0.08	3350	0.71	1.25	36.94	20.3	26.3	27.9
A2151	16 04 35.8	+17 43 18	31.47	+44.66	0.11	2800	0.64	1.10	36.72	20.5	26.5	27.9
A2152	16 05 29.3	+16 26 11	29.91	+43.99	0.11	2000	0.54	1.03	36.37	20.7	26.7	28.3

NOTE.—Columns list: cluster name; right ascension and declination (J2000) of the central galaxy; Galactic longitude and latitude of the central galaxy; R-band Galactic extinction in this direction (Schlegel et al. 1998); total LRIS exposure time in the final image (sec); full-width at half-maximum of the point spread function (arcsec); mean airmass; magnitude m_1^* of an object that would produce one source count per total integration time (see text); sky brightness in mag arcsec^{-2}; the 50% completeness limit for point source detection (mag; see text); and the expected R-band GCLF turnover magnitude.

were systematically off by $+0.07 \pm 0.02$ mag. This field has the highest galactic latitude and so is relatively devoid of stars. In addition, because of the cluster's distance and the need for a longer total integration, the individual exposures were twice as long as for the other fields with comparably good seeing, and stars with $m_R < 22.5$ were saturated. For these reasons, there were few good stars for doing absolute photometry in an automated way, and the empirical correction of 0.07 mag was applied to the magnitudes in this field.

As in BTM, a series of artificial star experiments were performed for each field to test the completeness limits of the point source detection and check for systematic biases in the recovered magnitudes as a function of magnitude. Composite stars were constructed and added in grids (so as to avoid artificial crowding while minimizing the number of separate tests required) to the images and then recovered with DOPHOT. The grid spacing was 30 pix, 20% larger than the PSF fit box. The tests proceeded in 10 or 11 steps of 0.4 mag, starting at $m_{\rm add} = 23.0$ or $m_{\rm add} = 23.4$. For each magnitude in each field, two separate DOPHOT runs were performed using grids offset with respect to each other by half a grid spacing in each direction. This allowed for better area sampling of the completeness function. Over 350,000 stars were added in 124 separate DOPHOT runs in the course of these experiments. The 50% detection completeness limits shown in Table 2 are the values determined from these tests at radii beyond $\sim 1'$ from the central galaxy. The number of real objects found by DOPHOT in these fields ranged from about 6,000 to nearly 10,000.

The results of these tests were used in choosing the cutoff magnitudes m_c for each field at which the point source detection completeness was 85–90% and any photometric bias in recovered magnitudes was negligible. As the completeness generally depends on radius, two or three different cutoff magnitudes were used for different radial regions in each field. Uncertainties in the completeness fraction $f_c \equiv {\rm N_{found}/N_{add}}$ were calculated as $\delta f_c = [f_c\,(1-f_c)/{\rm N_{add}}]^{1/2}$ (Bolte 1989) and included in the uncertainty estimated for the corrected counts. The final results for the counts due to GCs, corrected for incompleteness and background, are tabulated in Table 4 of §4.

3.2. *Radial Number Density Distributions*

After rejecting extended objects and correcting for incompleteness, the radial surface density of point sources in each field was fitted to a de Vaucouleurs $r^{1/4}$ law plus background model

$$N_{\rm ps}(r_p) \;=\; N(R_e) \times \exp[-7.67(r_p/R_e)^{1/4} - 1] + N_{\rm bg}\,, \quad (1)$$

where r_p is the projected radial distance (referenced this way to avoid confusion with the R magnitudes), R_e is the effective radius of the distribution, and $N_{\rm bg}$ is the background point-source level integrated over the magnitude range of the counts. The purpose of these fits was to estimate the backgrounds (primarily due to distant unresolved galaxies); the same approach was employed by BTM and previous authors (e.g., Harris 1986). The GC counts are then computed as $N_{\rm GC} = N_{\rm ps} - N_{\rm bg}$. Figures 7 through 12 show the radial distributions of the point sources found by DOPHOT to a completeness level of $\sim 90\%$ and the corresponding fits.

Many different radial binnings were explored for each field, and an average background value was chosen from among the fits. When the innermost points significantly changed the fit (due to a leveling off of the counts at small radii, as for A2152 in Fig. 12), they were excluded. Although one might consider adding other radial components to the model (for faint unresolved cluster dwarfs or a distinct population of intergalactic GCs), the quality of the fits ($\chi^2/N \sim 1$) does not warrant it. Any such additional components must be at a low level or have a spatial distribution extended enough to be nearly flat over the range of interest.

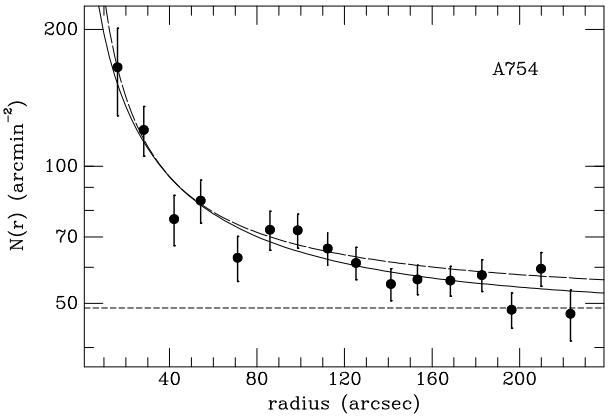

FIG. 7.— The incompleteness-corrected number density of point sources is plotted as a function of radial distance from the central galaxy in A754. The magnitude limits (corrected for Galactic extinction) for the counts are given in Table 3. The errorbars are dominated by the counting statistics but include some contribution from the uncertainty in the completeness. The plot is log-linear in order to better show the fractional uncertainty as a function of radius. The solid curve represents a 3-parameter de Vaucouleurs $r^{1/4}$ law fit to all the points shown; this fit was used to estimate the background point-source count level, shown as a horizontal short-dashed line. The background was then subtracted, and a 2-parameter power law was fitted to the points within a projected radius corresponding to $r < 105\,h^{-1}$ kpc (the uncertainty in the background was included in doing this fit). The long-dashed curve shows the best-fit power-law model with the background added back in.

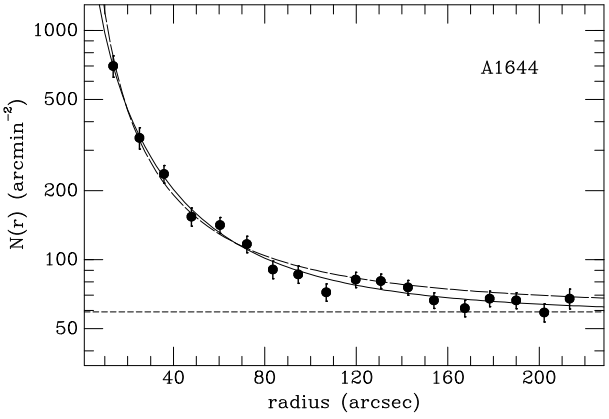

FIG. 8.— Same as Fig. 7, but for A1644.

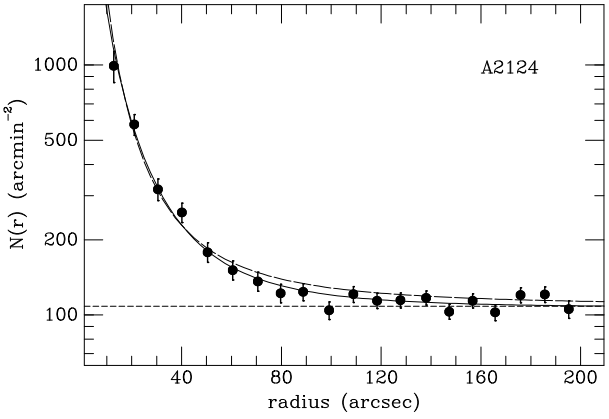

FIG. 9.— Same as Fig. 7, but for A2124.

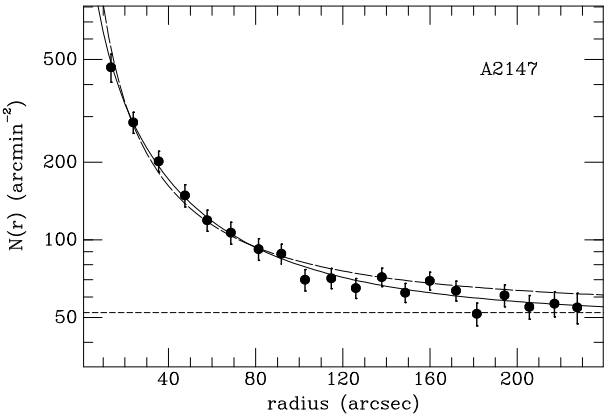

FIG. 10.— Same as Fig. 7, but for A2147.

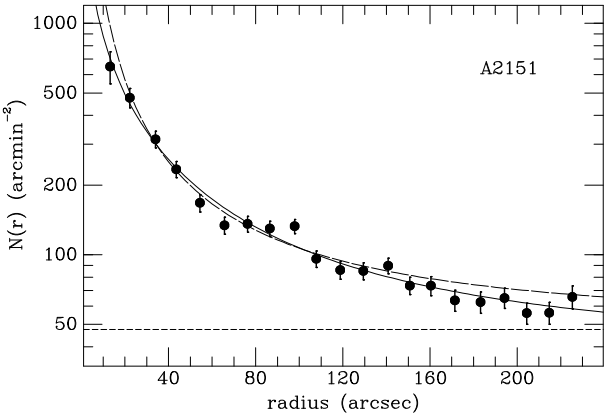

FIG. 11.— Same as Fig. 7, but for A2151.

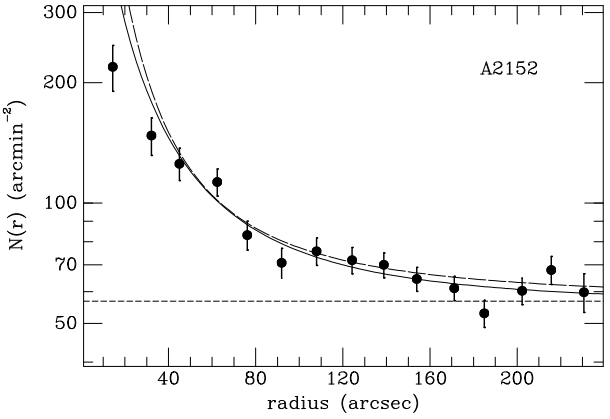

FIG. 12.— Same as Fig. 7, but for A2152. Note that the luminous SRG is within a radius of 50″.

The radial number densities of GCs in galaxy halos are also frequently parameterized as power laws of the form

$$N_{\rm GC}(r_p) \;=\; A_0 \times r_p^{\alpha}\,, \qquad (2)$$

where the power-law exponent is typically $\alpha \approx -1.5$ for gE's, but with a range from -1 to nearly -2.5 (e.g., Harris 1991; Kissler-Patig 1997). The background-subtracted surface densities of GCs for the present sample of galaxies

were fitted to power-law distributions of the above form. To aid in intercomparing the results, as well as to provide a better comparison for studies of more nearby galaxies, these power-law fits were done only within a radius corresponding to a projected distance of 105 h^{-1} kpc from the BCG centers. The fitted exponents are fairly insensitive to small changes in the magnitude or radial limits. These fits (with backgrounds added back in) are also displayed in Figures 7–12, and the parameters and magnitude range for each fit are listed in Table 3.

It is important to bear in mind that the GC distributions shown in the figures and characterized according to these simple radial forms actually encompass multiple cluster galaxies in each case. In particular for A754, A2151, and A2152 there are other bright galaxies in the fields with fairly significant GC populations. Specific frequencies are calculated below for the secondary galaxies in these three clusters. The galaxy 47″ northwest of the BCG in A2152 is comparable in luminosity to the BCG and has an obvious concentration of GCs; this is the main cause of the flattening of the surface density distribution at small radii in this cluster.

3.3. *Power Spectrum Measurements*

After all objects brighter than the chosen cutoff magnitude m_c are masked out of the image, the analysis proceeds by a Fourier-space measurement of the variance in surface brightness due to objects fainter than m_c remaining in the image. The power spectrum analysis is based on that used for the surface brightness fluctuations (SBF) method of determining galaxy distances (Tonry & Schneider 1988). A recent review of the SBF method is given by Blakeslee, Ajhar & Tonry (1999). The measured power spectrum $P(k)$ is modeled as a linear function of the "expectation power spectrum" $E(k)$, which is the convolution of the PSF with the window function of the mask,

$$P(k) \;=\; P_0 \times E(k) \;+\; P_1\,. \qquad (3)$$

The "white noise" component P_1 is well determined by the high wavenumbers, and so the problem becomes one of measuring the amplitude of the "fluctuation power" P_0. BTM and Tonry et al. (1990) discuss this measurement in detail and show example power spectra.

The P_0 fluctuation amplitude corresponds to the spatial variance in intensity from sources that have been convolved with the image PSF. It has contributions from GCs, faint galaxies, and the stellar SBF. The methods for estimating and subtracting the other contributions to obtain $P_{\rm GC}$, the fluctuation power due to GCs, were developed by Blakeslee & Tonry (1995) and have been discussed in more detail by BTM. The component due to the stellar SBF is estimated by scaling the nearby gE measurements, and the component due to faint galaxies is determined from the background galaxy luminosity function measured in the image. $P_{\rm GC}$ itself is directly proportional to the total surface density of GCs in the image, according to:

$$\begin{aligned} P_{\rm GC} \;&=\; \frac{N_0}{2} \times 10^{0.8(m_1^*-m^0+0.4\sigma_{\rm LF}^2\ln[10])} \\ &\times\; \mathrm{erfc}\left(\frac{m_c - m^0 + 0.8\sigma_{\rm LF}^2\ln[10]}{\sqrt{2}\,\sigma_{\rm LF}}\right) \end{aligned} \qquad (4)$$

(see Blakeslee & Tonry 1995), where N_0 is a normalization corresponding to the total number of GCs per unit area, m^0 is the turnover magnitude of the GCLF, and $\sigma_{\rm LF}$ is the Gaussian dispersion in magnitudes. The proportionality factor thus depends on the GCLF, but basically for elliptical galaxies when m_c is significantly brighter then m^0, then P_0 is always dominated by GCs rather than by the stellar SBF. (This ratio of fluctuation powers also depends on bandpass, as discussed by BTM.)

A new problem is created for the present data set by the variable PSF in the images. The measured P_0 is sensitive to the adopted PSF template used for $E(k)$. To test the reliability and robustness of the measured values, the fluctuation analysis was performed multiple times in each field using all the available high signal-to-noise, unsaturated stars in the region of the measurements as PSF templates (at least 3 per field). In addition, test reductions were done using composite PSF stars made by subrastering and adding $\sim$20 individual stars per frame, and then redone after spatially scaling the composite to have the same FWHM as found in the region of interest. In the end, one reduction that gave results near the median was chosen per field, and an allowance for an additional error of 6.25% was made in accordance with these tests to account for PSF mismatch. This additional uncertainty usually dominated the P_0 measurement error.

Table 4 presents all the P_0 measurements and estimated values of $P_{\rm GC}$, and §4 discusses how these are combined with the count information to constrain the GCLFs and total population sizes. First, however, the following section addresses one other correction that must be applied for the current data sample.

3.4. *Gravitational Lensing Corrections*

The clusters in this sample are of sufficient masses and distances that their gravity distorts the surface density of background sources. For this reason, the background level close to the BCG (assumed to be at the cluster center) may differ from that determined several arcminutes farther out. This effect is usually ignored in studies of GC systems in clusters. However, one of the sample clusters A2124 is known to possess a strongly lensed arc within a radius of 0.′5 of the BCG (Blakeslee & Metzger 1999). Although it is the most distant in the present sample, A2124 is less than a factor of two more distant than the nearest one, and it is not especially massive. Thus, lensing corrections were made for all the clusters as described below.

A cluster lens both magnifies the background sources and dilutes their surface density by some factor $A(r_p, z_\ell, z_s)$, where r_p is again the projected distance from the center of the mass distribution (assumed round), z_ℓ is the redshift of the lensing cluster, and z_s is the redshift of the source. (Broadhurst et al. [1995] and Trentham [1998] give fairly detailed discussions.) For lensing of *distant* sources by these clusters, $z_s \gg z_\ell \sim 0.05$, we can write the effect of the cluster on the background as:

$$N_{\rm g}'(m, r_p) \;=\; \frac{1}{A(r_p)}\, N_{\rm g}[m + 2.5\log A(r_p)] \qquad (5)$$

where $N_{\rm g}(m)$ would be the apparent magnitude distribution of distant galaxies in the absence of lensing, and we have assumed the sources lie at infinity and subsumed the

cluster redshift into the definition of $A(r_p)$. At the magnitudes of interest for the present analysis $m_R \gtrsim 25$, galaxies with luminosities $L \gtrsim 0.1\,L^*$ would lie at redshifts $z_s \gtrsim 1$. (In the end, we make a small correction for the finite redshift.)

As in BTM and Blakeslee & Tonry (1995), we assume a power-law galaxy magnitude distribution of the form

$$N_{\rm g}(m_R) \;=\; T_{\rm N} \times 10^{\,\beta\, m_R}\,, \tag{6}$$

where a slope of $\beta = 0.35$ is adopted for the R-band counts (Tyson 1988; Smail et al. 1995b; Hogg et al. 1997), consistent with the faint magnitude distributions in the present data set well away from the bright galaxies, and the normalization $T_{\rm N}$ is derived from the data. The lensing preserves the power-law form, and we can rewrite Eq. (5) as

$$\begin{aligned} N'_{\rm g}(m_R, r_p) &= [A(r_p)]^{-2.5(0.4-\beta)}\, N_{\rm g}(m_R) \\ &\equiv f_\ell(r)\, N_{\rm g}(m_R)\,, \end{aligned} \tag{7}$$

which defines the lensing correction factor $f_\ell(r)$. Since $A(r_p) > 1$ and $\beta < 0.4$ here, the surface density at a given apparent magnitude will be reduced by the lensing.

For a general lens, the magnification can be expressed as (see Miralda-Escudé 1991)

$$A \;=\; |(1-\kappa)^2 - \gamma^2|^{-1} \tag{8}$$

where κ and γ are the convergence and shear, respectively. The convergence is given by

$$\kappa \;=\; \Sigma(r_p) \left(\frac{c^2}{4\pi G} \frac{D_s}{D_\ell D_{\ell s}} \right)^{-1} \;\equiv\; \frac{\Sigma(r_p)}{\Sigma_{\rm crit}}\,, \tag{9}$$

where $\Sigma(r_p)$ is the surface mass density at a projected radius r_p, and we have used the general definition for the critical surface density $\Sigma_{\rm crit}$ in terms of the angular diameter distances from observer to source D_s, from observer to lens D_ℓ, and from lens to source $D_{\ell s}$. For an axisymmetric lens with the symmetry axis along the line of sight (i.e., an apparently round lens), the shear is

$$\gamma \;\equiv\; \frac{\overline{\Sigma}(r_p) - \Sigma(r_p)}{\Sigma_{\rm crit}}\,, \tag{10}$$

where $\overline{\Sigma}(r_p)$ is the mean surface density within r_p. Thus, for an assumed mass model $\Sigma(r_p)$, one can correct the background density using Eqs. (7)-(10).

Ideally, one would use deep multicolor (or redshift) information to select out background objects, then use shape information for a weak lensing analysis to constrain the mass distribution, and then determine the effect of this mass on the background surface density (extrapolated to fainter magnitudes). In practice, this would be extremely difficult because of the fairly low surface masses involved, the severe "contamination" of the background by cluster GCs, the small number of sources with measurable ellipticities, and the consequently coarse resolution of the weak-lensing maps. In any case, we lack multicolor or redshift information, and this level of detail is not necessary for present purposes.

Instead, the analysis explored a number of reasonable mass distributions ranging from a singular isothermal sphere having the cluster velocity dispersion, for which $\Sigma(r_p) = \frac{1}{2}\overline{\Sigma}(r_p) = (2Gr_p)^{-1}\sigma_{\rm cl}^2$, to more complicated models such as a superposition of a Hernquist (1990) model[1] for the cluster and an isothermal sphere with $\sigma_{\rm g} = 300$ km s^{-1} for the central galaxy. Isothermal models with cores were also explored. While X-ray studies find cluster core radii of $r_c = 100 \pm 50\ h^{-1}$ kpc (e.g., Forman & Jones 1999) lensing studies usually find much smaller values in the 20–40 h^{-1} kpc range, or less (Mellier et al. 1993; Miralda-Escudé 1995; Smail et al. 1995a; Tyson et al. 1998). For the case of A2124, Blakeslee & Metzger (1999) assumed the velocity dispersion in Table 1 and found a best-fit isothermal lensing model with $r_c \sim 10\ h^{-1}$ kpc. We chose to model all of the clusters as isothermal with a core radius $r_c = 20\ h^{-1}$ kpc. This gives lensing factors between the extremes of the singular isothermal and Hernquist models. A comparison of the predictions from different mass models suggests an uncertainty in the lensing factor (when integrated over the radial ranges used here) that is a third of the correction itself:

$$\delta f_\ell \;=\; \tfrac{1}{3}\,(1 - f_\ell)\,. \tag{11}$$

This is included in the uncertainty estimates for the lensing-corrected background counts.

The lensing correction to the background density gets as large as 27% ($f_\ell = 0.73 \pm 0.09$) for the innermost annulus (see the following section) of A2124. However, with the adopted $m_c = 26.1$ cutoff here, the pre-correction background is only $\sim$10% of the counts. Thus, the lensing correction changes the inferred number of GCs with $m_R < m_c$ by $\lesssim$3%. (In general, this correction has a slightly bigger effect on the counts than on the power spectrum results because the slope of the GC luminosity function at m_c is steeper than that of the galaxies.) Typical values of f_ℓ for this data set range from $\sim$0.84 for the innermost annulus to 0.98 for the outermost, but as the surface density of GCs falls with radius, the fractional effect on the inferred number is roughly the same. In the end, these corrections change the derived values for the total numbers of GCs by $\lesssim$5% and for the GCLF widths by $\sim$0.01–0.02 mag.

4. RESULTS

Table 4 collects all the point source counts, fluctuation measurements, and background estimates for all of the annular regions analyzed in each galaxy. These regions each extend a factor of two in radius, with the inner boundary of the innermost c1 region being 32 pix and the outer boundary of the outermost c4 region being 512 pix. We follow the identical χ^2 minimization procedure detailed by BTM. We assume the usual Gaussian form for the GCLF and simultaneously constrain the total numbers of GCs and the GCLF widths from the tabulated measurements. The expected GCLF mean (or turnover) magnitude m^0 is estimated for each cluster according to its velocity in the cosmic microwave background (CMB) rest

[1] A Hernquist model, or a Dehnen (1993) model with $\gamma = 1$, has a spatial mass density $\rho = \frac{M_{\rm tot}}{2\pi}\frac{a}{r}(r+a)^{-3}$. It is similar to a Navarro, Frenk & White (1996) model in that $\rho \sim r^{-1}$ at small radii, but has the advantage of being fully analytic. For the lensing calculations, these models were normalized by fixing the line of sight velocity dispersion to the tabulated values at $r_p = a$ and then a was varied within limits.

frame and the observed m_R^0 in the Virgo cluster. We use $m_R^0(\mathrm{Virgo}) = 23.2$ (from Ferrarese et al. 1999 and the colors of Ajhar et al. 1994) and assume an intrinsic scatter of 0.2 mag. This calibration is 0.05 mag brighter than that used by BTM, but we also revise the CMB velocity of Virgo to $1280 \pm 70\,\mathrm{km\ s^{-1}}$ so that the calculated values of m_R^0 (shown in Table 2) are consistent with those of BTM. With the mean Cepheid distance of 16.1 ± 0.3 Mpc for 5 Virgo spirals (Ferrarese et al. 1999), this gives $H_0 = 80$ km s^{-1} Mpc^{-1} for calculating the number of GCs per unit mass or luminosity. Changing the zero-point distance calibration would not affect the GCLF results, which depend only on the relative distance with respect to the Virgo cluster, and it would change the results for S_N and η_{GC} by only a constant factor, so the conclusions regarding general trends would not change. However, a systematic change in the distances with respect to Virgo *would* systematically change the GCLF results, and we check for this by comparing the results to the well-observed GCLF in Virgo. Such a change has only a small effect on the values for S_N and η_{GC}, since the inferred number of GCs changes in the same sense as the estimated masses and luminosities. BTM and §4.1 below discuss these issues further.

Tables 4 and 5 (below) report measurements for three galaxies besides the six BCGs in these clusters. A754-2 is 98″ away at a position angle PA = 80° from A754-1; A2151-2 is 92″ away at PA = 144° from A2151-1; and A2152-2 is 47″ away at PA = 302° from A2152-1. The point source counts and fluctuation analyses were done within annular regions centered around these three galaxies as well. Only the c1-c3 regions were analyzed for these; the circular region within 30″ of A2152-1 was masked out during the A2152-2 analysis (since these galaxies are so close together). Otherwise, very little attempt was made to protect against double counting of GCs between the pairs of galaxies. A2152-2 rivals A2152-1 in luminosity and was classified as the second ranked galaxy (SRG) in this cluster by Postman & Lauer (1995). The other two "secondary" galaxies are significantly fainter than the respective primary cluster galaxies, but they likewise had obvious concentrations of point sources around them.

4.1. *The GCLF, Biases, and Uncertainties*

Table 5 reports the results for the GCLF widths σ_{LF} and the specific frequencies S_N^{40} and S_N^{65} for different values of σ_{LF} derived within metric apertures of 40 and 65 kpc, respectively. The uncertainties in σ_{LF} include the effects of varying m_R^0 within the ± 0.22 mag uncertainty limits (derived from 0.2 mag intrinsic dispersion and a 0.1 mag random uncertainty in the cluster Hubble velocities). The weighted average (and the median) of the GCLF widths for all nine galaxies is $\langle\sigma_{\mathrm{LF}}\rangle = 1.54 \pm 0.03$ mag with an rms dispersion of 0.10 mag. The six BCGs give the same weighted average and dispersion with a median of 1.53 mag; if the A2124 BCG (the most distant in the sample) is excluded, the average is $\langle\sigma_{\mathrm{LF}}\rangle = 1.52 \pm 0.04$ mag with a dispersion of 0.08 mag.

BTM found $\langle\sigma_{\mathrm{LF}}\rangle = 1.45$ mag with a dispersion of 0.13 mag for their complete sample of 23 galaxies, but there was an apparent bias such that the most poorly determined σ_{LF} values were also the largest. When the 9 galaxies with the largest uncertainties were excluded, the mean was $\langle\sigma_{\mathrm{LF}}\rangle = 1.43$ mag with a dispersion of 0.07 mag. This result provided a good consistency check against M87, the central galaxy in Virgo and the main calibrator for the GCLF in these more distant clusters. Whitmore et al. (1995) found $\sigma_{\mathrm{LF}} = 1.44$ mag for their full sample of 1032 M87 GCs from Hubble Space Telescope (HST) imaging. The mean σ_{LF} for the present sample of BCGs is ~ 0.1 mag larger than these other values. Although this result is only marginally significant at the $\sim 2\sigma$ level, and values of $\sigma_{\mathrm{LF}} \gtrsim 1.55$ mag are not too uncommon in the literature (e.g., Madejsky & Rabolli 1995; Elson et al. 1998), we must consider the possibility that it is due to a systematic bias in the analysis.

If some systematic problem has caused σ_{LF} to be overestimated for the present sample, it is in the sense that the numbers derived from the counts are too high by $\sim 25\%$ with respect to those derived from the fluctuation analysis. For instance, BTM discussed the possibility that a population of unresolved dwarf galaxies clustering around the larger galaxies could masquerade as GCs. The implied properties of such dwarfs and the simulations of Bassino et al. (1994) led BTM to reject this as a serious problem. However, the potential for this problem would be greater in these richer, more distant clusters; it may be telling that the most distant cluster has the largest measured σ_{LF}. Future color information should help resolve this issue. BTM considered GCLF non-Gaussianity to be a bigger source of potential bias for σ_{LF} measurements. If the GCLF has enhanced tails with respect to a Gaussian, then the total number derived from the counts would be overestimated. Again, this problem is exacerbated when the cutoff magnitude for the counts is much brighter than the GCLF turnover, e.g., $m^0 - m_c \gtrsim 2.5$ mag. The small size of the current sample precludes any definitive determination of the presence of this effect. If it is true that the counts are simply overestimated due to contamination and/or that the extrapolation from the counts is too high because of non-Gaussianity, then the reported S_N values should be decreased by 5-10% (the fluctuation measurements carry more weight because of their smaller uncertainties).

A bias in σ_{LF} could also result from a systematic error in the m_1^* photometric zero points or in the m_R^0 values estimated from the redshifts. An error δm_R^0 or δm_1^* translates into a σ_{LF} error $\delta\sigma_{\mathrm{LF}} \approx \frac{1}{3}\delta m_R^0$ or $\delta\sigma_{\mathrm{LF}} \approx \frac{1}{3}\delta m_1^*$. Thus, the m^0 estimates or the m_1^* zero points would have to be wrong by 0.3 mag, in the sense that the data penetrate 0.3 mag further along the GCLF then we thought. External photometric comparisons rule out a photometric error of this size, and it is highly unlikely that the systematic error in m_R^0 could be this large, especially given the fact that BTM followed the same procedure. One change in the photometry for the present analysis is the use of *R*-band extinctions from Schlegel et al. (1998); the Burstein & Heiles (1984) extinctions for the program fields are less by 0.04-0.12 mag. Using the latter extinctions would decrease σ_{LF} by as much as 0.03 mag in the mean. However, it would have little effect on the result for A2124, the one with largest σ_{LF}, since this field has the smallest change in its estimated extinction.

Alternatively, the zero points and m_R^0 estimates could be correct, but the DoPhot magnitudes could be systematically off. The value of σ_{LF} is much more sensitive to this: an error δm_c in the assumed cutoff magnitude yields

an error $\delta\sigma_{\rm LF} \approx 2\,\delta m_c$. The reason is that Eq. (4) for the integrated number of GCs inferred from the fluctuations is a function of both $(m_1^*-m_R^0)$ and $(m_c-m_R^0)$, while the integrated number inferred from the bright counts is just a function of $(m_c-m_R^0)$. Changing the m_1^* zero point necessarily changes m_c as well, so the two sets of results change in similar ways. However, an independent error in m_c from the point-source photometry affects the two results differently, and so makes a bigger change in the value of $\sigma_{\rm LF}$. The tests described in §3.1 for absolute offsets in the aperture magnitudes, and for errors as a function of magnitude, indicate that $\delta m_c < 0.03$ mag (in the one case with a significant offset, a correction was made); thus, it does not appear that this could be the whole explanation. Perhaps several of the effects mentioned here contribute to a systematic increase in the average $\sigma_{\rm LF}$, although, again, it is marginal. The possibility of intrinsic variations in the GCLF is discussed in §5.4.

4.2. *Specific Frequencies*

Blakeslee (1997) introduced the "metric S_N" as the value of S_N calculated within a fixed metric radius of 40 kpc; we will refer to this quantity here as S_N^{40}. This approach removes the need for large and uncertain extrapolations to global values and reduces the risk of systematic errors with distance. Table 5 reported values of S_N^{40} for the six BCGs and the three other ellipticals mentioned above. The table shows how S_N^{40} decreases as $\sigma_{\rm LF}$ increases. Lacking clear evidence for intrinsic variations of $\sigma_{\rm LF}$ and in order to make the most homogeneous comparisons, we take the approach of BTM and assume a single value of $\sigma_{\rm LF} = 1.45 \pm 0.05$ mag for the whole sample.

Figure 13 shows S_N^{40} plotted against cluster velocity dispersion $\sigma_{\rm cl}$ for the present sample and the BTM sample. The BTM numbers have been decreased by 5% to correct for the slightly different distance scales used. We have also switched to $\sigma_{\rm cl} = 960$ km s^{-1} for the Coma cluster from Girardi et al. (1993) rather then the extreme "dense peak" value of 1140 km s^{-1} from Zabludoff et al. (1993). The correlation of S_N with $\sigma_{\rm cl}$ reported by Blakeslee (1997) and BTM persists, as the present sample of galaxies falls in line at the high-density/high-S_N end of the relation. The earlier sample also showed a strong increase in S_N with cluster X-ray properties; Figure 14 shows S_N^{40} plotted against X-ray luminosity in the 0.5–4.5 keV band for the combined sample. The new data again fit in at the high end of the relation. The quantitative relations minimizing the mean absolute deviations of the solid points in these two figures are given by:

$$S_N^{40} = 4.0 + 0.89 \times \left(\frac{\sigma_{\rm cl} - 415}{100}\right) \quad (12)$$

$$S_N^{40} = 4.0 + 2.24 \times (\log[L_{\rm X}] - 42.65)\,, \quad (13)$$

where $L_{\rm X}$ is in ergs s^{-1} and $\sigma_{\rm cl}$ is in km s^{-1}.

There is an important difference between the "secondary" galaxies in the BTM and present samples, represented by the different open symbols in Figures 13 and 14. The secondary galaxies in the BTM sample (shown as open circles) are gE's with luminosities similar to, and in some cases greater than, the primary central galaxies in their respective clusters. However, despite their great luminosities, they are removed from the dynamical and X-ray centers of the clusters. The secondary galaxies in the present sample (open stars) are lower luminosity ellipticals occupying the same central fields as the BCGs in these clusters. Thus, open circles represent high-luminosity non-central galaxies, while open stars represent low-luminosity central galaxies. If the number of GCs depends more on central location than on luminosity (as would be the case if there is a significant population of intracluster GCs), then one should expect the former galaxies to have lower specific frequencies than the latter galaxies, which in turn should have S_N values similar to those of the main central cluster galaxies. This is precisely what these figures show.

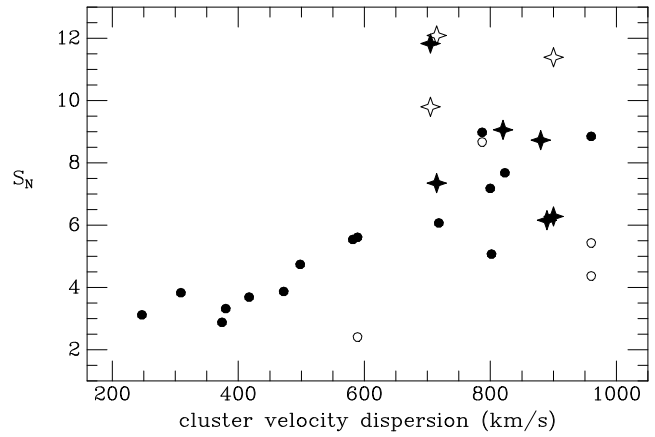

FIG. 13.— The correlation between GC specific frequency S_N and the velocity dispersion of the galaxies in the host cluster. Solid and open circles respectively represent the central and non-central ("secondary") cluster galaxies from the BTM sample. The solid four-pointed stars show the results for the main central cluster galaxies in the present sample, and the open stars are for other ellipticals in three of these same central fields. See text for details.

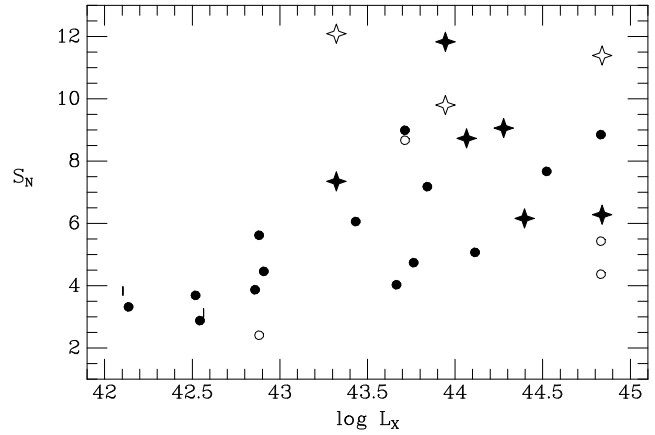

FIG. 14.— The correlation between GC specific frequency S_N and the X-ray luminosity of the host galaxy cluster. Symbols are as in Fig. 13, except for the short vertical lines which represent BTM galaxies in clusters with only upper limits on X-ray luminosity.

The larger area of the LRIS field of view and the greater distances of the present sample of galaxies allows S_N values to be measured over a larger range in radius. The last column of Table 5 lists values for S_N^{65}, the value of S_N within a metric radius of 65 kpc. These numbers provide better approximations to the global S_N values of the central cluster galaxies; the tabulated errors include uncertainties of ± 0.22 mag in m_R^0 and ± 0.05 mag in $\sigma_{\rm LF}$. The

general increase in S_N between 40 and 65 kpc indicates that the GC distributions are generally more extended than the halo light. There is nearly a factor of two variation in S_N among these galaxies, and although this sample as a whole fits in nicely at the high end of the S_N-density correlations, there is no such correlation apparent within this sample itself. Three of the BCGs have $S_N^{65} = 9$–10; the two most luminous ones have $S_N^{65} \sim 7$, and the A2151 BCG has $S_N^{65} = 12.5$. A2151 is only remarkable in being a fairly irregular, high spiral-fraction cluster; thus, it may be relatively young and dynamically unevolved. Possible implications of this observation are discussed in §5.3.

4.3. *GCs per Unit Mass*

Motivated by the increase in GC number with cluster density and the relative constancy of BCG luminosity which makes S_N depend on density, BTM defined the quantity $\eta_{\rm GC}$ as the number of GCs per unit mass: $\eta_{\rm GC} = N_{\rm GC}/M_{\rm cl}$, where $M_{\rm cl}$ here is the total mass in units of $10^9\,M_\odot$ within the same projected radius in which $N_{\rm GC}$ is measured. The procedure of using projected numbers and masses is analogous to calculating S_N from projected luminosity and number; Harris et al. (1998) take a different approach. The BTM $\eta_{\rm GC}$ parameter is similar to the T parameter defined by Zepf & Ashman (1993) as the number of GCs per unit mass for isolated galaxies.

Figure 15 shows $\eta_{\rm GC}$ calculated for the combined BTM plus present sample using two different cluster mass models. The top panel uses a singular isothermal model, for which $M(<r_p) = (\frac{\pi}{G})\sigma_{\rm cl}^2\, r_p$, and the lower panel uses the flat (projected) core model of BTM, for which $M(<r_p) \sim \sigma_{\rm cl}^{1.4}\, r_p^2$. Cohen & Ryzhov (1997) used the dynamics of the M87 GCs and found that the mass profile in Virgo was between these two cases. The masses are calculated between projected radii of ~ 4 kpc and 40 kpc, the range appropriate to the GC number. Thus, the "singular" isothermal model could be made to flatten within 4 kpc without changing the results. Because the present calculation now more properly excludes this central region, and because of the slightly longer distance scale used here, the BTM data points shown in the lower panel of the present Figure 15 are 6% higher than they were in BTM's own Figure 15, except for the Coma point, which is $\sim 30\%$ higher because it also uses a different velocity dispersion.

The isothermal model of the top panel gives $\eta_{\rm GC} \sim 0.5$ but probably overestimates the true mass; the flat core model of the lower panel gives $\eta_{\rm GC} \sim 0.9$ but likely underestimates the mass because it makes no account for a mass peak near the central galaxy. In either case, the scatter is about 30% and there is little trend left with $\sigma_{\rm cl}$. The highest point in both panels is A2151, which has the smallest velocity dispersion in the present sample; a dispersion more in line with its richness would lower its $\eta_{\rm GC}$. Without A2151, the scatter in $\eta_{\rm GC}$ for the flat core model would be closer to 20%, while the isothermal model would show a marginal decline in $\eta_{\rm GC}$ with $\sigma_{\rm cl}$. However, the isothermal model gives more consistent results with radius, since its projected mass density goes as r_p^{-1} and the GC surface densities in Figures 7–12 go as $\sim r_p^{-1.5}$. Table 6 lists the values of $\eta_{\rm GC}$ calculated within 40 and 65 kpc for each of the two mass models. The calculated $\eta_{\rm GC}$ drops by about 40% for the flat core model but only by about 10% for the isothermal model. Some drop would be expected if the total GC system is a combination of cluster and galaxy GC populations.

The new results are in good accord with those of BTM, who proposed that the apparent universality of $\eta_{\rm GC}$ (at least when calculated within a fixed metric radius) reflects a universal GC formation efficiency in the dense primordial environments that have become today's galaxy clusters. Thus, there remains no cause for invoking a density-dependent GC formation efficiency. The following section considers what light the present data shed on the formation, evolution, and luminosity functions of GC systems in clusters.

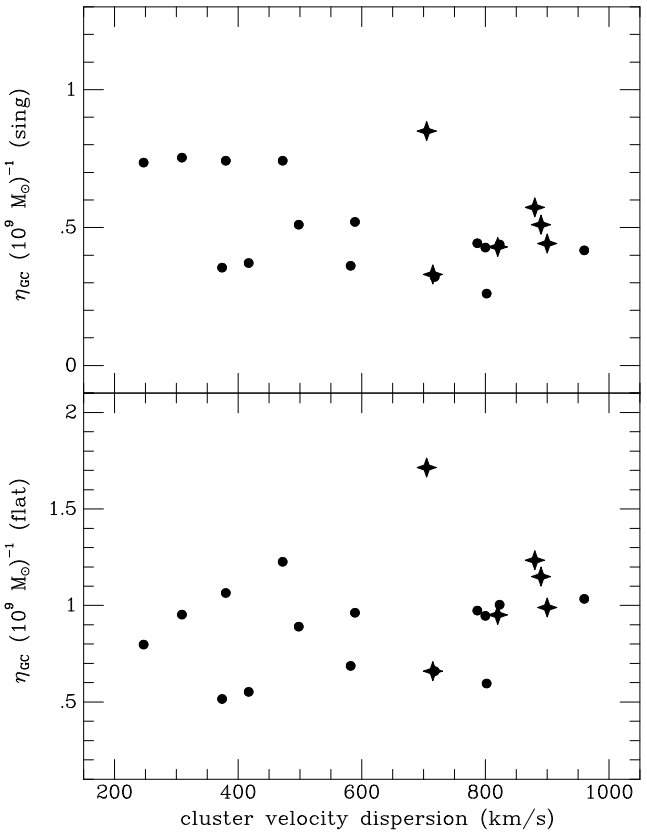

FIG. 15.— The number of GCs per unit mass η_{GC} is plotted against cluster velocity dispersion for the central cluster galaxies in the BTM (solid circles) and present (solid stars) samples. Both a singular isothermal model (top) and the flat core model of BTM (bottom) are used for estimating the masses. The average values in the two panels are 0.50 ± 0.16 and 0.93 ± 0.27 GC per $10^9\,M_\odot$, respectively.

5. DISCUSSION

As their numbers scale with overall properties of the galaxy clusters, the GCs of the central cluster galaxy might more correctly be called "cluster globulars" (or cluster GCs) as opposed to galactic ones (cf. West et al. 1995; BTM). Of course, it may be more appropriate to break the total population down into cluster and galactic components (e.g., Côté et al. 1998). This does not suppose that the putative cluster GC population formed outside of galaxies, as it is difficult to imagine that the very dense regions where the GCs must have originated did not eventually become galaxies. However, these galaxies would be "cluster galaxies"; thus, all of their associated GCs would have the potential to become "cluster globulars," whether

through early escape during the relaxation of the protogalaxy, by later stripping during interactions, or by falling into the center of the potential well during cluster collapse to help form the dominant galaxy there.

5.1. *Universal Formation Efficiencies*

McLaughlin (1999b) contends that his view of the universal GC formation efficiency is "quite different" from that of BTM, and thus different from the one given here. His main point of contention is that BTM estimated efficiencies in terms of the number of GCs per unit total mass, instead of using only the combined mass of the stars and gas, i.e., the "baryonic mass." BTM used the most convenient observable at hand to estimate masses, namely the cluster velocity dispersion. No mention of the role of nonbaryonic dark matter was made in that work, apart from the statement that this approach obviated the need for ill-constrained assumptions such as dark matter biasing or a density-dependent efficiency.

McLaughlin (1999b) is incorrect in stating that the BTM efficiencies were computed using the total masses of the "*entire* galaxy clusters" (italics his). Rather, the masses were estimated within the identical projected radii in which the numbers of GCs were measured (since we can only observe clusters in projection). If the GCs, which are known to scale with cluster properties, roughly follow the mass distribution, then the results computed within projected radii will be similar to those found within three-dimensional radii. In addition, the universal efficiencies proffered by BTM and McLaughlin will be equivalent, modulo a scale factor equal to the ratio of the masses used. In a different work, McLaughlin (1999a) concludes that the mass distribution of the hot gas follows the overall dark matter distribution, at least at large radii. He quotes a ratio of the gas mass to dark matter mass in Virgo of $\rho_{\rm gas}/\rho_{\rm DM} \sim 0.035$. Thus, to convert between the different efficiencies, we need now only to estimate the ratio of the stellar and gas masses over the range in projected radii for which the GC surface densities were measured, i.e., from ~ 4 to 40 kpc.

For the gas, we adopt the Hernquist (1990) mass model from McLaughlin (1999a,b) to obtain a projected mass $M_{\rm gas} = 1.77 \times 10^{11}\,{\rm M}_\odot$ over this range in projected radius. To estimate the stellar mass, we use a Hernquist model having the same effective radius $R_{\rm e} = 7.0$ kpc as the photometry used by McLaughlin (de Vaucouleurs & Nieto 1978), which extends out to ~ 100 kpc. We normalize the model such that the spatial mass density of the stars $\rho_\star(r)$ equals that of the gas $\rho_{\rm gas}(r)$ at $r = 42$ kpc (McLaughlin 1999b). This yields $M_\star = 4.28 \times 10^{11}\,{\rm M}_\odot$ for this projected radial range; the appropriate projected mass ratio is then $M_\star/M_{\rm gas} = 2.4$. The identical value is obtained if one instead uses the McLaughlin (1999a) mass model for the stellar distribution (a $\gamma = 1.33$ Dehnen model). Thus the appropriate ratio of total to baryonic projected mass is

$$\begin{aligned} M_{\rm tot}/(M_{\rm gas}{+}M_\star) &= (M_{\rm gas}{+}M_\star{+}M_{\rm DM})/(M_{\rm gas}{+}M_\star) \\ &\approx (1 + 2.4 + 0.035^{-1})/(1 + 2.4) \\ &\approx 9.4\,. \end{aligned} \tag{14}$$

The average of the values for the GC mass rate $\eta_{\rm GC}$ from the two panels of Figure 15 is

$$\eta_{\rm GC} \;=\; 0.71 \pm 0.22 \;\; {\rm GC}\; M_\odot^{-9}\,.$$

This is similar to the value quoted by BTM, so we will work with it. To convert this to a dimensionless efficiency, we adopt a mean individual GC mass of $\langle m_{\rm GC}\rangle = 2.4 \times 10^5\,{\rm M}_\odot$, as in McLaughlin (1999b). The inferred GC formation efficiency per unit total mass is then $\epsilon_{\rm tot} = (1.71 \pm 0.53) \times 10^{-4}$. Using Eq. (14) to convert this to an efficiency per unit baryonic mass, we obtain $\epsilon_{\rm b} = 0.0016 \pm 0.0005$. The errorbar here should be considered a rough lower limit on the uncertainty, which may be nearer to $\sim 50\%$, given the fairly crude mass models employed. In any case, this result is close to McLaughlin's proposed universal value of $\epsilon_{\rm b} = 0.0026 \pm 0.0005$.

McLaughlin (1999a) remarks on the similarity of the total stellar and gas masses which makes the baryon fraction $M_{\rm b}/M_{\rm DM} \sim 0.07$. He also notes that the dark matter distribution is not constrained for $r \lesssim 15$ kpc. In the model of Harris et al. (1998), the strong galactic winds that removed the star-forming gas from the proto-cD would have left the dark matter distribution intact, as this material is supposed to interact only gravitationally. Taking the view of Waxman & Miralda-Escudé (1995), Navarro et al. (1996), and Aragón-Salamanca, Baugh, & Kauffmann (1998) that the dark matter is *more* centrally concentrated than the hot gas, and thus more closely follows the overall baryonic mass distribution, we find $\epsilon_b \approx (1{+}0.07^{-1}){\times}1.71{\times}10^{-4} = 0.0026$, fortuitously identical to the McLaughlin value.

Given these considerations, McLaughlin's universal GC formation efficiency appears identical in every palpable way to that of BTM, who presented the initial observational evidence for it and made a rough first estimate of its value. (The idea itself goes back at least twenty years to Harris & Petrie [1978].) McLaughlin's work has substantially refined the idea and allowed for significant progress on the physical mechanisms underlying the observations.

5.2. *GC Color Distributions*

Up to now, this discussion has ignored the vast wealth of recent data on the color distributions of GC populations (e.g., Ostrov et al. 1993; Whitmore et al. 1995; Geisler et al. 1996). The complex, often bimodal GC color distributions of gE galaxies must surely be important clues bespeaking a complex enrichment history. The situation is simpler for dwarf ellipticals, which appear to have only metal poor GCs (see Côté et al. 1998). In hierarchical formation models, giant galaxies are constructed (at early times for dense environments) through chaotic merging of numerous smaller subunits that must have resembled dwarf galaxies (e.g., Searle & Zinn 1978). To be consistent with observations, the gE progenitors must have formed their high metallicity GCs during this process; several lines of argument suggest this is possible (see Ashman & Zepf 1992). The final GC metallicity distribution will be broader and more metal rich than that of the dwarf progenitors, but in a continuous hierarchical collapse, there is no *a priori* reason to expect distinct metallicity peaks or a change in S_N to occur. Côté et al. (1998) have demonstrated using realistic galaxy luminosity functions that later dissipationless mergers can result in gE's having bimodal GC distributions, again without any change in S_N.

In any case, the similarity in the GC color distributions of cD galaxies and more ordinary ellipticals (Forbes et al. 1997) reinforces the conclusion of BTM that there is nothing special, or unusual, about the GCs around central cluster galaxies. For instance, the GC color distributions in M87 and M49 in Virgo are both bimodal in appearance, despite the fact that M87's S_N is about 3 times higher. Kissler-Patig et al. (1999) pointed out that the similarity between the GC color distributions of the Fornax cD NGC 1399 and the other Fornax ellipticals is expected, despite NGC 1399 having an S_N twice that of any of the others, if S_N increases by a simple transfer of GCs through tidal stripping. However, stripping scenarios in virialized clusters have unsolved problems with time scale (Muzzio 1987), and it is not at all clear that S_N should increase, since both stars and GCs will be added (e.g. Harris 1991), although it might (e.g., Côté et al. 1998).

5.3. *BCG Formation and the Evolution of S_N*

Since both the GC color distributions and numbers per unit mass are normal in high-S_N galaxies, the question is one of the missing light: why do these galaxies lack the halo light necessary to bring their specific frequencies and mass-to-light ratios down to normal levels? Motivated by the "standard candle" aspect of BCGs (e.g., Postman & Lauer 1995), BTM suggested that the collapse of the galaxy cluster tidally heated and removed the gas from the central galaxy and halted star formation there. Improvements in numerical modeling of BCG formation can help to refine this idea.

Recent simulations indicate that giant central galaxies form on relatively short time scales during the initial collapse of the cluster. Garijo, Athanassoula, & García-Gómez (1997) simulated the formation of central galaxies in clusters with a variety of different initial conditions. They observed rapid growth of a central dominant galaxy and the early formation of an extended halo of debris. The cD obtained a great mass within 1 Gyr for their higher velocity dispersion clusters. Dubinski (1998) studied the collapse and evolution of a 550 km s^{-1} dispersion cluster in a hierarchical formation simulation starting at $z=2$ and found that the most massive galaxies all merged together to form one central object in less than 3 Gyr (by $z=0.8$). Some other galaxies were subsequently accreted, but there were no more large mergers in the cluster center after $z=0.4$.

Unfortunately, the simulations do not yet include modeling of the gas dynamics and star formation in the collapse. Starbursts would likely occur during the rapid series of mergers, but arguing that GCs must have formed at a higher than normal rate in some clusters (relative to the total number of stars formed) does not solve the problem, which results from "missing light," or "luminosity saturation," not "excess globulars." If the simulations are correct that massive central galaxies form quickly, and more quickly in the more massive protoclusters, then the simple assumptions that, (1) most GCs are older than most stars, and (2) the central galaxy quickly loses the cool gas necessary to form stars, are sufficient to explain the observations. The first of these assumptions is true in our own Galaxy, and spectroscopy of a large sample of M87 GCs indicates that they are uniformly old as well (Cohen et al. 1998). The second assumption is true today except in rare cases ($\sim 4\%$, according to Lauer & Postman 1994). Aragón-Salamanca et al. (1998) conclude from BCG colors out to $z\sim 1$ that no significant star formation has taken place in BCGs since that epoch; they suggest that the gas is less centrally concentrated than the dark matter, and hence unable to cool efficiently enough to form stars.

Both tidal heating (BTM) and strong, starburst-driven galactic winds (Harris et al. 1998) during the cluster-collapse/BCG-formation epoch have been offered as means for removing gas from the BCG. The faster formation of BCGs in denser (simulated) environments would drive the gas out sooner. As an example, assume that the GCs formed first on a fixed short time scale, so that their total number is proportional to the mass in an isothermal model: $N_{\rm GC} \sim M_{\rm cl} \sim \sigma_{\rm cl}^2$. Also assume that the amount of material for forming non-GC stars has this dependence, but that the time $t_\star$ available for forming the stars is inversely proportional to the velocity dispersion: $N_\star \sim M_{\rm cl} t_\star \sim \sigma_{\rm cl}$. Thus,

$$S_N \sim N_{\rm GC}/N_\star \sim \sigma_{\rm cl}\,, \tag{15}$$

and we reproduce a linear dependence as in the empirical relation given by Eq. (12). A more elaborate scenario awaits further advances in the simulations, but an analogy can be drawn with the situation in the Milky Way. If we assume that 90% of Galactic stars formed after the GCs did and use the *current* mass-to-light ratio $(M_\star/L_V)_0$ of the Galactic stellar population to compute $S'_N(t)$, a "corrected" specific frequency at that early time, then

$$S'_N(t) \;=\; \frac{N_{\rm GC}}{M_\star(t)/(M_\star/L_V)_0} \;\approx\; 10\,S_N(t_0)\,, \tag{16}$$

where $S_N(t_0) \approx 0.5$ (Harris 1991) is the Galactic S_N today. This is simply meant to illustrate that after the formation of the Galactic GCs and before the gas settled down to form stars in the disk, the relative amount of stellar mass in GCs was greater. In this sense, S_N (i.e., S'_N) was higher at early times and has decreased because of star formation.

Of course, even if very few stars form in the cluster center after collapse, star formation will continue in other cluster galaxies as in the Milky Way; given enough time, the central galaxy will accrete enough stars (and some GCs too) to decrease its S_N (without affecting $\eta_{\rm GC}$). McLaughlin et al. (1994) called this proces S_N "dilution" and suggested that they saw evidence for it in a possible correlation between S_N and BM type. Improved measurements and larger samples (Ostrov et al. 1998; BTM) fail to support this trend, but this may be because BM type is not a robust measure of evolutionary state. In addition, kinematical studies of the galaxies within cluster centers indicate that the current merger rate extrapolated over a cluster lifetime will increase the BCG luminosity by only $\sim 1L^*$ (Merrifield & Kent 1991; Blakeslee & Tonry 1992), consistent with the estimates of Merritt (1985), although Aragón-Salamanca et al. (1998) find a higher rate from the K-band Hubble diagram for BCGs out to $z\sim 1$, approaching the cluster formation epoch.

The time scale for such S_N dilution will be shortest in highly compact, low-dispersion clusters such as Fornax. (Indeed, given the recent precipitous drop in published values of S_N for NGC 1399, one might conclude it was on the order of years.) BTM puzzled over Fornax because

its supposed high-S_N cD did not fit in with the observed correlations. However, two revised estimates both give $S_N = 3.9 \pm 0.6$ (Ostrov et al. 1998; Kissler-Patig et al. 1999), where we have corrected to the mean Cepheid distance $(m-M) = 31.40$ (Ferrarese et al. 1999) found for two Fornax spirals. Thus NGC 1399 now agrees well with the relation given by Eq. (12), for instance. However, the predominance of the cD halo in this galaxy and the correlation of S_N with the extendedness of the light distribution (BTM) makes it reasonable to hypothesize that NGC 1399 originally had a higher S_N which has decreased through cluster dynamical evolution. There is evidence from X-ray data (Jones et al. 1997) that nearby NGC 1404 is in the process of being accreted; when this occurs, NGC 1399's S_N will drop by 10% (see Kissler-Patig et al. 1999).

Finally, returning to the present sample of galaxies, we ask if there is any evidence for S_N evolution here. The sample covers the spectrum of morphological type. Usually differences in cluster richness obscure any effects that might be associated with morphological state, but here the six clusters are fairly similar in richness. As noted earlier, the A2151 BCG has the highest $S_N = 12.5$ and also a spiral fraction near 50%, indicating a significant amount of ongoing star formation in this cluster. The A2152 BCG and its close neighbor, which together constitute a binary BCG, have high values of S_N given that the X-ray properties show A2152 to be the poorest in the sample. The richest cluster is A754, which unexpectedly has the lowest $S_N = 6.8$, but its morphology and the BCG's high luminosity suggest that the cluster is well evolved. Similarly, the A1644 BCG's S_N would increase to ~ 10 if its luminosity were about the mean for this sample. Thus, we may be beginning to see the effects of central galaxy luminosity evolution causing a decrease in S_N, although much work is needed before this can be confirmed.

5.4. *The GCLF and Cluster Distances*

BTM noted that their results were consistent with the GCLFs in their sample clusters being scaled versions of the M87 GCLF translated in distance; this supported the idea of a universal GCLF for cluster gE's. In contrast, the recent work of Ferrarese et al. (1999) warns against using the GCLF as a distance indicator because the V-band GCLF is intrinsically brighter by 0.5 ± 0.1 mag in the Fornax poor cluster than in Virgo, based on their Cepheid distances and published GCLF measurements. The situation for the B-band is even worse: the GCLF is brighter by 0.64 ± 0.25 mag in Fornax, and by nearly 1.2 mag in the Leo group, than in Virgo. Blakeslee & Tonry (1996) earlier noted this trend and proposed that it was due to environmental effects; as further evidence, they pointed to the then preliminary HST results indicating that the GCLF in the richer Coma cluster was significantly *fainter* than in Virgo. In fact, the results of Baum et al. (1997) do indicate that the GCLF is fainter by 0.4 ± 0.2 mag in Coma than in Virgo when compared to the relative distances from most other methods (e.g., van den Bergh 1992; Jerjen & Tammann 1993; D'Onofrio et al. 1997; Kelson et al. 1999). As all of the measurements are for ellipticals, the problem cannot be solved by invoking different GCLFs for different Hubble types.

Ferrarese et al. (1999) note that the Coma HST data do not adequately sample the GCLF turnover and thus conclude the result is unreliable. Moreover, the BTM results are more consistent with the GCLF being the same in Coma as in Virgo. The difference of ~ 0.1 mag noted in §4.1 between the mean $\sigma_{\rm LF}$ of the present sample and that of M87 is in the wrong sense—the GCLF would have to be *brighter* by ~ 0.3 mag in these dense clusters than in Virgo and the BTM clusters (although still fainter than in Fornax). Thus, while ellipticals in poor groups appear to have intrinsically brighter GCLFs than those in clusters, there is no strong evidence for further variation in the GCLF among clusters over a very large range in richness.

If we assume that the GCLF is universal for BCGs, we can use a restricted form of the GCLF distance method for the sample galaxies. Instead of fixing m_R^0 from the CMB velocity and constraining $\sigma_{\rm LF}$, we can fix $\sigma_{\rm LF}$ to some value and vary m_R^0 until the point source and fluctuation measurements give the same answer for the total number of GCs; thus we obtain an estimate of the relative cluster distances. Of course, this approach is subject to all the same potential problems from reaching unequal depths along possibly non-Gaussian GCLFs. That said, we note that five of the BCGs have $\sigma_{\rm LF}$ consistent with the median of 1.53 mag, while the A2152 BCG has $\sigma_{\rm LF} = 1.36$ mag. This assumes that distance goes as redshift $d \sim z$ (from Barmby & Huchra 1998) so that A2152 is 30 Mpc behind the other two Hercules supercluster members A2147 and A2151. Requiring the A2152 $\sigma_{\rm LF}$ to be ~ 0.15 mag larger to match the others gives a distance 23% larger than implied by its redshift, so that A2152 is ∼60 Mpc in the background and falling towards the supercluster with a peculiar velocity near 2500 km s^{-1}. Given the uncertainties and the sensitivity of m_R^0 on changes in $\sigma_{\rm LF}$, this "Hercules infall" is clearly not a significant result, and we continue to prefer the assumption that redshift reflects distance.

On the positive side, the GCLF analysis does indicate that A2152 is not likely to be at the same distance as the other two Hercules clusters and falling away from us at high speed through the "plane" of the supercluster. If we do assume that it is at the same distance, then its $\sigma_{\rm LF}$ drops to 1.24 ± 0.10 mag, which is significantly less than that of any of the other clusters, as well as less than for any of the 23 BTM galaxies. (Some galaxies, including M31 [Secker 1992], do have GCLFs this narrow or narrower, but none among this large sample of similar galaxies.) Thus, this restricted form of the GCLF method, requiring both the mean and the dispersion to be universal for BCGs, implies that A2152 is significantly behind the other two supercluster members, consistent with the mean redshifts from Barmby & Huchra (1998) and in contrast to previous works that found roughly equal mean redshifts for all three clusters (e.g., Zabludoff et al. 1993). It would be worth trying to disentangle this triple cluster system with more robust methods such as the fundamental plane or Tully-Fisher.

6. SUMMARY AND CONCLUSIONS

Deep LRIS R-band imaging has been presented for the centers of six rich Abell clusters, all with velocity dispersions $\sigma_{\rm cl} > 700$ km s^{-1}. We have used both the counts of point sources as a function of radius and the residual fluctuations in surface brightness after the removal of these point sources to study the GC populations around the central cluster galaxies. New features necessary for the

analysis of the present data set include allowances for a spatially varying PSF and small corrections to the background surface densities for gravitational lensing effects. The point source counts give somewhat higher values for the extrapolated total numbers of GCs, if the width of the GCLF is $\sigma_{\rm LF} \sim 1.4$; we have offered several reasons why the counts might be biased high. Alternatively, if there is no such bias, we have measured a median $\sigma_{\rm LF} = 1.53$ mag. This is about 0.1 mag broader than that found for the BTM sample of galaxies in generally lower-mass clusters. A restricted application of the GCLF distance method indicates that A2152 is likely more distant than the rest of the Hercules supercluster.

The correlations found by BTM for S_N with velocity dispersion and X-ray luminosity continue to hold up for these rich clusters. We have provided empirical scaling relations for S_N in the combined data set. The derived values for the number of GCs per unit mass $\eta_{\rm GC}$ are similar to those found for the BTM sample; the implied "universal" GC formation rate is $\eta_{\rm GC} \sim 0.5$–1 GC per $10^9\,M_\odot$. Thus, the variation seen in S_N with cluster mass seems to result from "missing light" rather than anything unusual in the number of GCs. The GC color distributions found by other authors in central cluster galaxies lend further support to this view.

Guided by recent numerical simulations of BCG formation, we have argued that the observations are explained by a scenario in which the GCs formed at early times and fell into the cluster center along with their associated galaxies which merged to form the BCG. In this process of cluster collapse and BCG formation, the gas may have become heated and lost to the intracluster environment (BTM, Harris et al. 1998) so that star formation ceased early in the cluster center. Although the simulations do not yet predict the star formation rates, they indicate that the BCG formation process is more rapid in richer clusters, consistent with the above scenario for producing higher-S_N, higher-M/L central galaxies in these clusters.

Over the subsequent lifetime of the cluster, a high-S_N central galaxy will slowly grow in luminosity and evolve towards lower S_N. In particular, continuing star formation in the general galaxy population of a young, spiral-rich cluster may allow the central galaxy to grow more luminous without the addition of a significant number of new GCs. We have suggested that the available data are beginning to show the first evidence for such evolution: the most spiral-rich, irregular cluster in our sample has the BCG with highest S_N, and the most centrally concentrated, apparently well-evolved clusters have BCGs with lower values of S_N and higher luminosities.

I wish to thank Judy Cohen, Bev Oke, and the rest of the team responsible for producing the Low Resolution Imaging Spectrograph. I thank Pat Côté for reading and commenting on the manuscript, Mark Metzger for his help with DoPhot, John Tonry for the use of much software, and Judy Cohen for helpful comments throughout this work. G. Kochanski made some enlightening comments at the AAS Meeting in Austin, and Terry Stickel provided excellent assistance at the telescope. I also thank the anonymous referee for helpful comments and corrections. This research has made use of the NASA/IPAC Extragalactic Database (NED), which is operated by the Jet Propulsion Laboratory at Caltech, under contract with the National Aeronautics and Space Administration. I gratefully acknowledge the financial support of a Sherman M. Fairchild Fellowship.

REFERENCES

Abell, G. O., Corwin H. G. Jr. & Olowin, R. P. 1989, ApJS, 70, 1
Ajhar, E. A., Blakeslee, J. P., & Tonry, J. L. 1994, AJ, 108, 2087
Aragón-Salamanca, A., Baugh, C. M., & Kauffmann G. 1998, MNRAS, 297, 427
Ashman, K. M. & Zepf, S. E. 1992, ApJ, 384, 50
Barmby, P. & Huchra, J. P. 1998, AJ, 115, 6
Bassino, L. P., Muzzio, J. C., & Rabolli, M. 1994, ApJ, 431, 634
Baum, W. A. 1955, PASP, 67, 328
Baum, W. A., Hammergren, M., Thomsen, B., Groth, E. J., Faber, S. M., Grillmair, C. J., & Ajhar, E. A. 1997, AJ, 113, 1483
Blakeslee, J. P. 1997, ApJ, 481, L59
Blakeslee, J. P., Ajhar, E. A., & Tonry J. L. 1999, in Post-Hipparcos Cosmic Candles, eds. A. Heck & F. Caputo (Dordrecht: Kluwer Academic Publishers), 181
Blakeslee, J. P. & Metzger, M. R. 1999, ApJ, 513, 592
Blakeslee, J. P. & Tonry, J. L. 1992, AJ, 103, 1457
Blakeslee, J. P. & Tonry, J. L. 1995, ApJ, 442, 579
Blakeslee, J. P. & Tonry, J. L. 1996, ApJ, 465, L19
Blakeslee, J. P., Tonry, J. L., & Metzger, M. R. 1997, AJ, 114, 482 (BTM)
Bolte, M. 1989, ApJ, 341, 168
Broadhurst, T. J., Taylor, A. N., & Peacock, J. A. 1995, ApJ, 438, 49
Burstein, D. & Heiles, C. 1984, ApJS, 54, 33
Cohen, J. G., Blakeslee, J. P. & Ryzhov, A. 1998, ApJ, 496, 808
Cohen, J. G. & Ryzhov, A. 1997, ApJ, 486, 230
Côté, P., Marzke, R. O., & West, M. J. 1998, ApJ, 501, 554
Dehnen, W. 1993, MNRAS, 265, 250
de Vaucouleurs, G. & Nieto J.-L. 1978, ApJ, 220, 449
D'Onofrio, M., Capaccioli, M., Zaggia, S. R., & Caon, N. 1997, MNRAS, 289, 847
Dressler, A. 1980a, ApJS, 42, 565
Dressler, A. 1980b, ApJ, 236, 351
Dubinski, J. 1998, ApJ, 502, 141
Elson, R. A. W., Grillmair, C. J., Forbes, D. A., Rabban, M., Williger, G. M., & Brodie, J. P. 1998, MNRAS, 295, 240
Fadda, D., Girardi, M., Giuricin, G., Mardirossian, F., Mezzetti, M. & Biviano, A. 1996, ApJ, 473, 670
Ferrarese, L. et al. 1999, ApJ, submitted (H_0 Key Project Paper XXVI)
Forbes, D. A., Brodie, J., & Grillmair, C. J. 1997, AJ, 113, 1652
Garijo, A., Athanassoula, E., & García-Gómez, C. 1997, A&A, 327, 930
Geisler, D., Lee, M. G., & Kim, E. 1996, AJ, 111, 1529
Girardi, M., Biviano, A., Giuricin, G., Mardirossian, F., & Mezzetti, M. 1993, ApJ, 404, 38
Harris, W. E. 1986, AJ, 91, 822
Harris, W. E. 1991, ARA&A, 29, 543
Harris, W. E., Harris, G. L. H., & McLaughlin, D. E. 1998, ApJ, 115, 1801
Harris, W. E. & Petrie, P. L. 1978, ApJ, 223, 88
Harris, W. E., Pritchet, C. J., & McClure, R. D. 1995, ApJ, 441, 120
Harris, W. E. & Pudritz, R. E. 1994, ApJ, 429, 177
Harris, W. E. & van den Bergh, S. 1981, AJ, 86, 1627
Hernquist L. 1990, 356, 359
Hill, J. M. & Oegerle, W. R. 1993, AJ, 106, 831
Hogg, D. W., Pahre, M. A., McCarthy, J. K., Cohen, J. G., Blandford, R., Smail, I., & Soifer, B. T. 1997, MNRAS, 1997, 288, 404
Jerjen, H. & Tammann, G. A. 1993, A&A, 276, 1
Jones, C. & Forman, W. 1999, ApJ, 511, 65
Jones, C., Stern, C., Forman, W., Breen, J., David, L., Tucker, W., & Franx, M. 1997, ApJ, 482, 143
Kelson, D. D. et al. 1999, ApJ, submitted (H_0 Key Project Paper XXVII)
Kissler-Patig, M. 1997, A&A, 319, 83
Kissler-Patig, M., Grillmair, C. J., Meylan, G., Brodie, J. P., Minniti, D., & Goudfrooij, P. 1999, AJ, 117, 1206
Landolt, A. U. 1992, AJ, 104, 340

Lauer, T. R. & Postman, M. 1994, ApJ, 425, 418
Madjesky, R., & Rabolli, M. 1995, A&A, 297, 660
McLaughlin, D. E., Harris, W. E., & Hanes, D. A. 1994, 422, 486
McLaughlin, D. E. 1999a, ApJ, 512, L9
McLaughlin, D. E. 1999b, AJ, 117, 2398
Mellier, Y., Fort, B., & Kneib, J.-P. 1993, ApJ, 407, 33
Merrifield, M. R. & Kent, S. M. 1991, AJ, 101, 783
Merritt, D. 1985, ApJ, 289, 18
Metzger, M. R. & Schechter, P. L. 1998, AJ, 116, 469
Miralda-Escudé, J. 1991, ApJ, 370, 1
Miralda-Escudé, J. 1995, ApJ, 438, 514
Muzzio, J. C. 1987, PASP, 99, 245
Navarro, J. F., Frenk, C. S., & White, S. D. M. 1996, ApJ, 462, 563
Oemler, A. 1976, ApJ, 209, 693
Oke, J. B., Cohen, J. G., Carr, M., Cromer, J., Dingizian, A., Harris, F. H., Labrecque, S., Lucinio, R., Schaal, W., Epps, H., & Miller, J. 1995, PASP, 107, 307
Ostrov, P., Geisler, D., & Forte, J. C. 1993, AJ, 105, 1762
Ostrov, P., Forte, J. C. & Geisler, D. 1998, AJ, 116, 2854
Postman, M. & Lauer, T. R. 1995, ApJ, 440, 28
Schlegel, D., Finkbeiner, D., & Davis, M. 1998, ApJ, 500, 525
Schechter, P. L., Mateo, M., & Saha A. 1993, PASP, 105, 1342
Schombert, J. M. 1988, ApJ, 328, 475
Searle, L. & Zinn, R. 1978 ApJ, 225, 357
Secker, J. 1992, AJ, 104, 1472
Smail, I., Hogg, D. W., Blandford, R., Cohen, J. G., Edge, A. C., & Djorgovski, S. G. 1995a, MNRAS, 277, 1
Smail, I., Hogg, D. W., Yan, L., & Cohen, J. G. 1995b, ApJ, 449, 108
Struble, M. F. & Rood, H. J. 1987, ApJS, 63, 555
Struble, M. F. & Rood, H. J. 1991, ApJS, 77, 363
Tarenghi, M., Chincarini, G., Rood, H. J., & Thompson, L. A. 1980, ApJ, 235, 724
Tonry, J. L., Ajhar, E. A., & Luppino, G. A. 1990, AJ, 100, 1416
Tonry, J. L. & Schneider, D. P. 1988, AJ, 96, 807
Trentham, N. 1998, MNRAS, 295, 360
Tyson, J. A. 1988, AJ, 96, 1
Tyson, J. A., Kochanski, G. P., & Dell'Antonio, I. P. 1998 ApJ, 498 L107
van den Bergh, S. 1992, PASP, 104, 861
Waxman, E. & Miralda-Escudé, J. 1995, ApJ, 451, 451
West, M. J. 1993, MNRAS, 265, 755
West, M. J., Côté, P., Jones, C., Forman, W., & Marzke, R. O. 1995, ApJ, 453, L77
Whitmore, B. C., Sparks, W. B., Lucas, R. A., Macchetto, F. D., & Biretta, J. A. 1995, ApJ, 454, L73
Whitmore, B. C. 1996, in The Extragalactic Distance Scale, eds. M. Livio, M. Donahue, & N. Panagia, (Cambridge: Cambridge University Press)
Zabludoff, A. I., Geller, M. J., Huchra, J. P., & Ramella, M. 1993, AJ, 106, 1273
Zabludoff, A. I. & Zaritsky, D. 1995, ApJ, 447, L21
Zepf, S. E. & Ashman, K. M. 1993, MNRAS, 264, 611

Captions for GIF images of program fields:

FIG. 1.— Center of the Keck LRIS *R*-band image of Abell 754. North is up; East is to the left.

FIG. 2.— Center of the Keck LRIS *R*-band image of Abell 1644. North is up; East is to the left.

FIG. 3.— Center of the Keck LRIS *R*-band image of Abell 2124. North is up; East is to the left.

FIG. 4.— Center of the Keck LRIS *R*-band image of Abell 2147. North is up; East is to the left.

FIG. 5.— Center of the Keck LRIS *R*-band image of Abell 2151. North is up; East is to the left.

FIG. 6.— Center of the Keck LRIS *R*-band image of Abell 2152. North is up; East is to the left.

TABLE 3
POWER-LAW FITS TO GC RADIAL NUMBER DENSITY DISTRIBUTIONS

Field	m_b, m_c	$R_{\max}$	$\log A_0$	$\pm$	α	$\pm$
A754	23.0, 25.6	$140''$	3.29	0.32	−1.02	0.22
a1644	23.0, 26.0	$160''$	4.62	0.13	−1.56	0.09
a2124	23.6, 26.6	$120''$	5.22	0.20	−1.96	0.16
a2147	22.5, 25.6	$215''$	4.29	0.13	−1.40	0.10
a2151	22.5, 25.8	$205''$	4.48	0.12	−1.35	0.09
a2152	22.5, 26.0	$175''$	4.62	0.54	−1.66	0.34

NOTE.—Table lists for each cluster: the bright and faint limiting R-band magnitudes m_b, m_c of the background-corrected point source counts used for the fit; radius corresponding to 105 h^{-1} kpc out to which the fits were done; base-ten logarithm of the best-fit scale factor A_0 (which has units of number/arcmin^2/arcsec$^\alpha$) and its uncertainty; and best-fit power-law exponent α and its uncertainty.

TABLE 4
POINT SOURCE COUNTS AND VARIANCE MEASUREMENTS

Galaxy.reg	m_b	$N_{\rm ps}$	$\pm$	f_ℓ	$N_{\rm GC}$	$\pm$	m_c	P_0	$\pm$	$P_{\rm GC}$	$\pm$
A754-1.c1	23.0	175.7	106.4	0.77	146.4	106.5	25.4	1152	179	1026	180
A754-1.c2	23.0	110.1	17.9	0.85	77.7	18.5	25.4	637	46	503	49
A754-1.c3	23.0	92.6	7.9	0.93	48.1	9.8	25.6	353	24	236	28
A754-1.c4	23.0	68.9	3.5	0.98	22.3	6.9	25.6	183	14	62	20
A1644-1.c1	23.0	383.2	69.1	0.80	357.1	69.1	25.6	2182	142	1999	144
A1644-1.c2	23.0	267.3	32.4	0.86	239.1	32.5	25.6	1279	83	1104	85
A1644-1.c3	23.0	194.1	11.8	0.94	139.1	12.2	26.0	418	28	300	30
A1644-1.c4	23.0	101.7	4.1	0.98	44.5	5.0	26.0	227	15	107	19
A2124-1.c1	23.6	641.6	125.2	0.73	595.8	125.3	26.1	2675	241	2446	243
A2124-1.c2	23.6	390.7	37.1	0.85	323.0	37.4	26.3	1287	102	1087	104
A2124-1.c3	23.6	235.9	13.4	0.94	133.4	13.8	26.6	431	29	276	32
A2124-1.c4	23.6	124.1	4.4	0.98	17.4	5.4	26.6	196	13	36	19
A2147-1.c1	22.5	322.2	70.1	0.88	287.9	70.1	25.3	1195	121	1086	122
A2147-1.c2	22.5	261.2	25.4	0.91	222.2	25.5	25.4	555	40	467	42
A2147-1.c3	22.5	131.9	9.4	0.95	91.1	9.7	25.4	326	21	240	26
A2147-1.c4	22.5	90.3	3.9	0.98	38.8	5.0	25.6	143	9	72	15
A2151-1.c1	22.5	211.0	62.6	0.92	193.9	62.6	25.0	1241	88	1143	88
A2151-1.c2	22.5	285.2	31.0	0.93	258.3	31.2	25.4	553	39	490	39
A2151-1.c3	22.5	252.9	13.3	0.96	207.4	14.2	25.8	186	12	145	13
A2151-1.c4	22.5	130.7	4.6	0.99	84.2	6.7	25.8	92	6	51	7
A2152-1.c1	22.5	112.3	32.9	0.90	86.0	33.0	25.5	192	16	165	16
A2152-1.c2	22.5	153.7	21.2	0.92	101.7	21.6	26.0	55	5	40	5
A2152-1.c3	22.5	130.6	9.7	0.96	76.5	10.5	26.0	38	3	23	4
A2152-1.c4	22.5	86.4	3.8	0.99	31.0	5.7	26.0	23	2	8	2
A754-2.c1	23.0	296.3	141.8	0.98	258.9	141.9	25.4	784	180	632	181
A754-2.c2	23.0	89.2	15.9	0.98	51.9	16.6	25.4	389	28	239	34
A754-2.c3	23.0	66.6	6.6	0.98	19.8	8.9	25.6	194	26	72	29
A2151-2.c1	22.5	175.7	40.2	0.99	157.3	40.3	25.0	725	65	623	65
A2151-2.c2	22.5	153.8	20.6	0.99	125.3	20.9	25.4	262	18	198	19
A2151-2.c3	22.5	141.3	9.7	0.99	94.6	10.8	25.8	110	7	69	8
A2152-2.c1	22.5	169.8	44.7	0.97	141.5	44.8	25.5	207	17	180	17
A2152-2.c2	22.5	224.8	26.8	0.97	170.3	27.1	26.0	63	5	48	5
A2152-2.c3	22.5	127.9	10.2	0.97	73.4	11.0	26.0	35	2	20	3

NOTE.—For each annular region of each galaxy, the table lists: bright cutoff magnitude m_b of the point source counts; incompleteness-corrected number of point sources $N_{\rm ps}$ (arcmin^{-2}) fainter than m_b but brighter than m_c; the lensing factor f_ℓ that was applied to the background estimate; total number of GCs $N_{\rm GC}$ (arcmin^{-2}) in the m_b-m_c magnitude range; faint cutoff m_c; fluctuation power P_0 from objects fainter than m_c, in units of 10^4 (e^-/pixel)^2; the power $P_{\rm GC}$ due to GCs fainter than m_c, also in 10^4 (e^-/pixel)^2.

TABLE 5
RESULTS FOR $\sigma_{\rm LF}$ AND S_N

Galaxy	M_V^{40}	$\sigma_{\rm LF}$	±	($\sigma_{\rm LF}$= 1.4) S_N^{40}	+ −	($\sigma_{\rm LF}$= 1.5) S_N^{40}	+ −	($\sigma_{\rm LF}$= 1.6) S_N^{40}	+ −	M_V^{65}	S_N^{65} + −
A754-1	−22.87	1.54	0.10	6.8	0.5	5.8	0.4	4.9	0.4	−23.31	$6.8\,^{2.3}_{1.7}$
A1644-1	−23.04	1.60	0.09	6.5	0.3	5.8	0.3	5.2	0.2	−23.36	$7.0\,^{2.0}_{1.6}$
A2124-1	−22.71	1.64	0.14	9.3	0.5	8.2	0.4	7.3	0.4	−23.00	$9.9\,^{2.9}_{2.3}$
A2147-1	−22.30	1.53	0.09	9.6	0.5	8.6	0.4	7.7	0.4	−22.67	$9.8\,^{2.8}_{2.2}$
A2151-1	−22.42	1.50	0.09	12.5	0.5	11.2	0.4	10.1	0.4	−22.85	$12.5\,^{3.4}_{2.7}$
A2152-1	−21.92	1.36	0.10	7.8	0.5	6.9	0.5	6.1	0.4	−22.19	$9.1\,^{2.7}_{2.1}$
A754-2	−21.36	1.72	0.22	12.3	1.9	10.6	1.6	9.2	1.4	...	...
A2151-2	−21.62	1.55	0.11	10.3	0.6	9.4	0.5	8.6	0.5	...	...
A2152-2	−21.43	1.47	0.11	12.7	0.8	11.5	0.7	10.4	0.7	...	...

NOTE.—Columns list for each galaxy: absolute V-band magnitude M_V^{40} projected within 40 kpc (h=0.8); best-fit Gaussian width $\sigma_{\rm LF}$ of the GC luminosity function (mag); metric specific frequencies S_N^{40} within projected radii of 40 kpc and their internal errors for $\sigma_{\rm LF}$ values of 1.40, 1.50, and 1.60 mag; absolute V-band magnitude M_V^{65} projected within 65 kpc; and metric specific frequencies S_N^{65} and total uncertainties within projected radii of 65 kpc ($\sigma_{\rm LF} = 1.45 \pm 0.05$).

TABLE 6
ESTIMATES OF GCs PER MASS

	singular		flat core	
Cluster	$\eta_{\rm GC}^{40}$	$\eta_{\rm GC}^{65}$	$\eta_{\rm GC}^{40}$	$\eta_{\rm GC}^{65}$
A754	0.44	0.42	0.99	0.60
A1644	0.51	0.45	1.15	0.66
A2124	0.57	0.48	1.23	0.68
A2147	0.43	0.38	0.95	0.54
A2151	0.85	0.78	1.71	1.01
A2152	0.33	0.31	0.66	0.39

NOTE.—The second and third columns give the number of GCs per unit $10^9\,M_\odot$ within 40 and 65 kpc, respectively, as estimated from a singular isothermal cluster model. The last two columns give the same quantities but estimated from a flat core model as in BTM.